JOURNAL OF GEOPHYSICAL RESEARCH, VOL. 116, B04102, doi:10.1029/2010JB007843, 2011

A Preisach method for estimating absolute paleofield intensity under the constraint of using only isothermal measurements: 1. Theoretical framework

Adrian R. Muxworthy[1] and David Heslop[2,3]

Received 13 July 2010; revised 13 July 2010; accepted 14 January 2011; published 8 April 2011.

[1] The theoretical framework for a new nonheating method of determining absolute ancient magnetic field intensities (paleointensities) is described. The approach is based on a thermally activated Preisach model for interacting, randomly orientated single-domain grains with uniaxial anisotropy. The model includes theoretical features not accommodated by previous nonheating paleointensity methods; for example, it includes magnetostatic interactions, allows for variable cooling rates, and can identify, isolate, and reject unstable remanence carriers, i.e., multidomain and superparamagnetic contributions. The input Preisach distribution from which the acquisition of a thermal remanent magnetization (TRM) of a given rock sample can be simulated is obtained from information contained in the sample's first-order reversal curve distribution. The paleointensity estimate is determined by comparing the alternating field demagnetization spectrum of the sample's natural remanent magnetization and its simulated TRM. In the companion paper, the protocol is rigorously tested using a suite of historical samples.

Citation: Muxworthy, A. R., and D. Heslop (2011), A Preisach method for estimating absolute paleofield intensity under the constraint of using only isothermal measurements: 1. Theoretical framework, *J. Geophys. Res.*, *116*, B04102, doi:10.1029/2010JB007843.

1. Introduction

[2] Recovering the absolute value of the ancient magnetic field intensity (paleointensity) recorded by rocks has proven to be problematic since the first attempts were made [*Folgerhaiter*, 1899; *Koenigsberger*, 1938a, 1938b; *Thellier*, 1941]. The original methods assumed that the natural remanent magnetization (NRM) was essentially a thermoremanent magnetization (TRM). By comparing the NRM of a rock with a laboratory-induced TRM, the ancient field strength was estimated by simple scaling with the laboratory field. The main drawback of this direct approach is that the heating that is required to induce the laboratory TRM, will often chemically alter the magnetic minerals in a rock. This means the NRM and TRM are not comparable and would yield an incorrect paleointensity estimate. To identify chemical alteration, *Koenigsberger* [1938a, 1938b], *Thellier* [1941], and *Thellier and Thellier* [1959] introduced a stepwise thermal remagnetization protocol for paleointensity determination, which was modified by *Coe* [1967] to include double demagnetization/remagnetization steps at increasing temperatures until a full TRM is induced. This "Thellier-type" approach of *Coe* [1967] and its many subsequent modifications form the basis of most modern paleointensity studies. While the Thellier-type experiments provide a method with which to identify laboratory chemical alteration according to certain empirical criteria, the detection of such alteration only serves as a mechanism for rejecting samples, which are deemed to be unsuitable for paleointensity analysis.

[3] For the stepwise approach of the Thellier-type methods to work, it is required that the samples obey the law of partial TRM (pTRM) additivity [*Dunlop and Özdemir*, 1997]; that is, a stepwise TRM (a pTRM) acquired over the temperature T_1 and T_3 should be equal to the sum of two pTRMs acquired over the temperature range T_1 to T_2 and T_2 to T_3, respectively, and reciprocity, i.e., blocking and unblocking temperatures are equal [*Xu and Dunlop*, 2004]. The laws of additivity and reciprocity are obeyed by small magnetically single-domain (SD) grains, but larger multidomain (MD) grains violate them [*Dunlop*, 1998]. The contribution of intergrain magnetostatic interactions has not been quantified rigorously, and it is still debated if interacting SD grains will obey these laws or not [*Levi*, 1977; *Fabian*, 2001; *Dunlop et al.*, 2005]. These requirements present major problems for many rocks types, which contain a wide grain size spectrum of magnetic particles spanning the SD to MD states.

[4] Violation of pTRM additivity and reciprocity, and the effects of chemical alteration during the experiment can lead

[1]Department of Earth Science and Engineering, Imperial College London, London, UK.
[2]Fachbereich Geowissenschaften, Universität Bremen, Bremen, Germany.
[3]Now at Research School of Earth Sciences, Australian National University, Canberra ACT, Australia.

0148-0227/11/2010JB007843

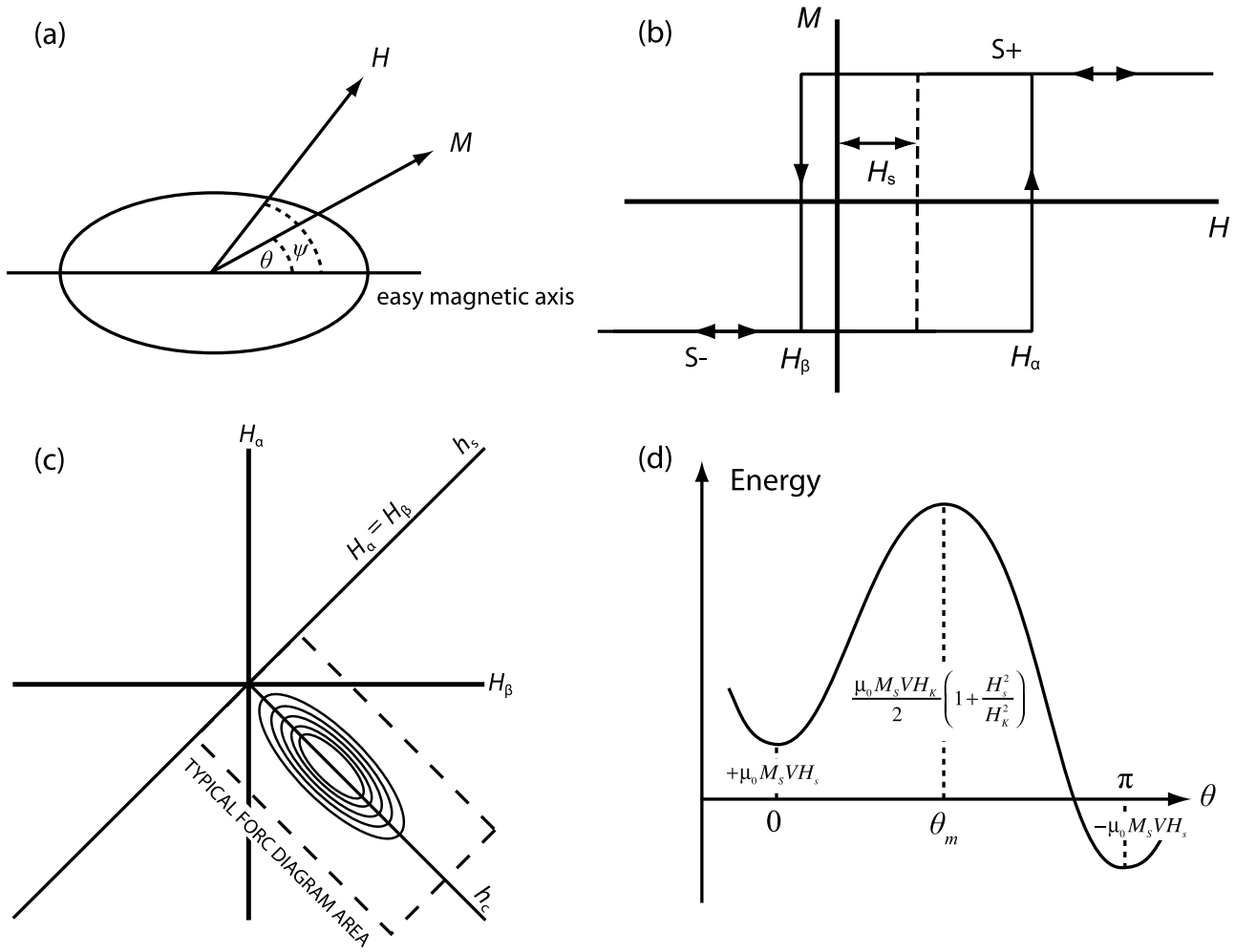

Figure 1. (a) A Stoner-Wohlfarth (SW) particle with the easy magnetic axis, applied field (H) and magnetization (M) direction highlighted. In SW particles the magnetization lies in the same plane as the anisotropy field plane. (b) Hysteresis loop for a SW particle with $\psi = 0°$. The hysteresis loop, or hysteron, is shifted by the variable H_s field associated with interactions (equation (3)). (c) A schematic representation of the Preisach plane and the relationship between the various field parameters discussed in the text with the position of a typical first-order reversal curve (FORC) diagram included. (d) The energy barrier experienced by the hysteron in Figure 1b; θ_m is the position of the energy maximum, ΔE_C.

to very high sample rejection rates in Thellier-type experiments. For example, *Paterson et al.* [2010] performed Thellier-type paleointensity investigations on a total of 129 samples from two localities, which ultimately did not yield a single reliable paleointensity estimate. Such high rejection rates are a particular issue given the very time-consuming nature of Thellier-type experiments.

[5] Alternatives to Thellier-type protocols do exist, such as the *Shaw* [1974] method, the microwave method [*Walton et al.*, 1993], and the multispecimen parallel differential pTRM method [*Dekkers and Böhnel*, 2006]. These methods are expected to suffer less from the effects of chemical alteration but are not immune because they all still involve sample heating to some extent.

[6] Nonheating methods have been developed to study the magnetic fields in the early Solar System, as the materials used in such studies, i.e., chondrules found in primitive chondrites, are particularly vulnerable to chemical alteration during Thellier-type experiments [*Gattacceca and Rochette*, 2004]. These nonheating remanence (REM) methods and their modifications, compare the NRM normalized by some laboratory-induced isothermal remanence with calibration charts, essentially yielding calibrated relative paleointensity estimates [e.g., *Fuller et al.*, 1988; *Kletetschka et al.*, 2000; *Gattacceca and Rochette*, 2004]. The REM method and its variants do not truly account for intrinsic variation in the magnetic mineralogy and domain state, and as such are estimated by *Gattacceca and Rochette* [2004] to only be accurate to at best a factor of 2.

[7] There is a clear need for more accurate nonheating paleointensity methods. Here and in the companion paper [*Muxworthy et al.*, 2011], we describe a new nonheating method of paleointensity determination based on Preisach theory [*Preisach*, 1935]. The basic premise behind the new

approach is that in using Preisach models it is possible to predict the response of a magnetic system to variations in both magnetic field and thermal activation energy [*Bertotti*, 1998; *Mayergoyz*, 2006], and temperature [*Stancu and Spinu*, 1998; *Roshko and Viddal*, 2004]. If we know the Preisach distribution of a sample, it is possible to make a predictive estimate of its TRM (NRM) intensity for a given field strength. Another advantage of using Preisach models, is that according to *Néel*'s [1953] first-order interpretation, Preisach distributions provide a description of magnetostatic interactions. No previous paleointensity method has theoretically accommodated magnetostatic interactions, which may be critical, although it is uncertain whether interactions cause pTRM additivity laws to be violated [*Levi*, 1977; *Shcherbakov et al.*, 1995; *Fabian*, 2001; *Dunlop et al.*, 2005].

[8] In this paper we describe the theory behind the proposed methodology, and *Muxworthy et al.* [2011] report an empirical test of the method on over 275 samples from modern lavas and pyroclastic lithics. Of these samples, 252 are less than 100 years old and the geomagnetic field is accurately known at the time of eruption.

2. A Thermally Activated Preisach Model

[9] The theoretical framework for the model developed in this paper is adapted primarily from the temperature- and time-dependent Preisach-Néel models of *Stancu and Spinu* [1998] and *Roshko and Viddal* [2004] for *Stoner and Wohlfarth* [1948] particles. For completeness, we will review briefly the basic ideas of these models in addition to our own developments; to aid comparison with the existing literature, we have adopted the nomenclature of *Stancu and Spinu* [1998].

2.1. Aligned Stoner-Wohlfarth particles

[10] The free energy of a uniaxial Stoner-Wohlfarth (SW) particle with an external magnetic field H is given by

$$E = KV\sin^2\theta - \mu_0 M_S H V\cos(\psi - \theta) \tag{1}$$

where K is the anisotropy constant, V is the volume of the particle, μ_0 is the permeability of free space, M_S is the spontaneous magnetization, θ is the angle between the M_S direction and the easy axis, and ψ is the angle between the external field and the easy axis direction (Figure 1a).

[11] For the case where $\psi = 0°$, the heights of the energy barriers ($\Delta E_\pm$) separating the stable magnetization directions can be derived from equation (1) [*Stoner and Wohlfarth*, 1948; *Néel*, 1949]:

$$\Delta E_\pm = \frac{\mu_0 M_S V}{2H_K}(H_K \pm H)^2 \tag{2}$$

where H_K (= $2K/\mu_0 M_S$) is the anisotropy field, which is equal to the switching field H_C for the case $\psi = 0°$. The positive sign signifies rotation out of the external field direction, and the negative sign corresponds to rotation into the field direction.

[12] In the classical Preisach model for a system of SW particles with their easy axes aligned with the field direction ($\psi = 0°$), the magnetic moment of each particle is described by a single point in the Preisach plane that has coordinates H_α and H_β corresponding to the switching fields of the hysteron shown in Figure 1b. The effective magnetic field acting on the particle is the sum of the applied field H_a and the interparticle interaction field H_{int}, which is taken to be aligned with the field direction. The interaction field thus translates the rectangular hysteresis loop along the field axis by a value $H_s = -H_{int}$ (Figure 1b). The effective field experienced by the hysteron is therefore given by

$$H = H_a + H_{\text{int}} = H_a - H_s \tag{3}$$

The total magnetization, M, for a distribution $p(H_\alpha, H_\beta)$ of such particles experiencing a range of interaction fields (Figure 1c) is simply

$$M = \int_{S+} p(H_\alpha, H_\beta)\,dH_\alpha dH_\beta - \int_{S-} p(H_\alpha, H_\beta)\,dH_\alpha dH_\beta \tag{4}$$

where S+ and S− represent hysterons in the positive and negative states, respectively.

[13] The SW model does not take thermal fluctuations into account, and therefore, in the classical Preisach model the magnetic moment cannot overcome energy barriers (equation (2)) in effective fields less than the switching fields. The effect of thermal fluctuations can be included using *Néel*'s [1949] model, which describes the relaxation of the magnetic moment over a given energy barrier ΔE:

$$\tau = \tau_0 \exp\left(\frac{\Delta E}{k_B T}\right) \tag{5}$$

where τ is the characteristic time for thermal activation, τ_0^{-1} is the atomic attempt frequency, k_B is Boltzmann's constant, and T is the absolute temperature. For a two-state model with relaxation times, τ_+ and τ_- the relaxation process is described by

$$\frac{1}{\tau} = \frac{1}{\tau_+} + \frac{1}{\tau_-}$$

where

$$\tau_\pm = \tau_0 \exp\left(\frac{\Delta E_\pm}{k_B T}\right) \tag{6}$$

It is apparent that if $\tau_+ \gg \tau_-$, then $\tau = \tau_-$ and vice versa. In combination with the strong field dependency of $\tau_\pm$, this means that $\tau_\pm$ is effectively the duration, t, of the given time frame of interest, e.g., will barriers be overcome on geological timescales, the duration of a laboratory experiment.

[14] The critical barrier height ΔE_C (Figure 1d) separates those barriers that are spontaneously overcome ($\Delta E < \Delta E_C$) from those which are not ($\Delta E > \Delta E_C$); that is, for an applied field, H_a, particles will relax to their equilibrium state if

$$\frac{\mu_0 M_S V}{2H_K}\left(H_K \pm (H_a - H_s)^2\right) < k_B T \ln\left(\frac{t}{\tau_0}\right) \tag{7}$$

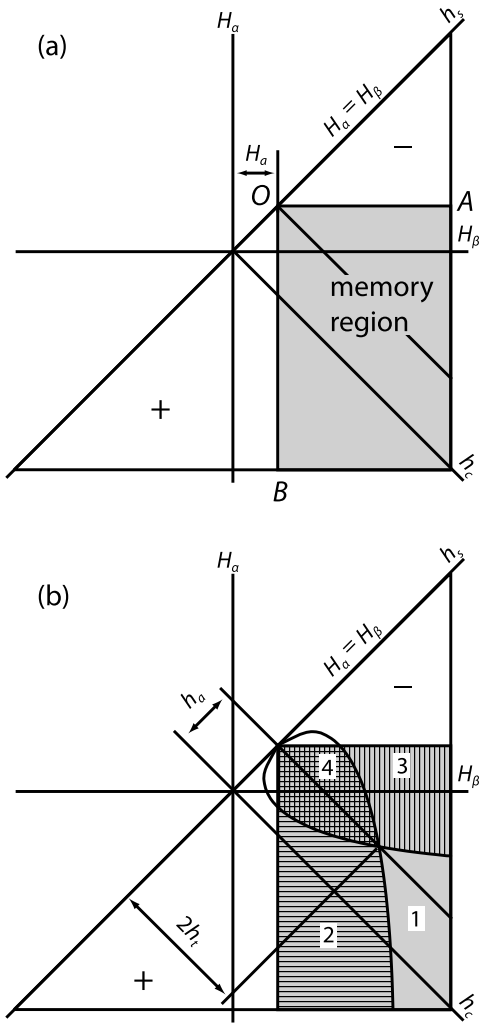

Figure 2. (a) Preisach diagram in the absence of thermal energy, i.e., at 0 K the "field blocking regime," showing the effect of the applied field on the three regions marked positive (plus), negative (minus), and memory. The positive and negative regions are field blocked and retain no record of their magnetic history; that is, the hysterons in these regions are in their positive and negative states, respectively. The memory region (shaded box) incorporates hysterons that can be either positive or negative depending on their history. (b) A thermally activated Preisach diagram, i.e., $T > 0$ K. The thermal critical barriers (equation (11)) now split the memory region into four zones; zone 1 is still capable of retaining a record of its history, i.e., thermally blocked region, whereas in zones 2–4 the thermal energy is now sufficient for the energy barriers in (Figure 1c) to be overcome; that is, these regions are superparamagnetic. Note that the shape of the critical barriers is dependent on ψ; for the example shown we have set $\psi = 0°$.

The representation of the thermally induced switching in the Preisach plane can be expressed using thermal critical curves given by

$$(H_K \pm (H_a - H_s))^2 = 2H_K H_T$$

where

$$H_T = \frac{k_B T}{\mu_0 M_S V} \ln\left(\frac{t}{\tau_0}\right) \tag{8}$$

Transforming to the Preisach coordinate system (h_c, h_s), which is rotated by 45° with respect to the (H_α, H_β) system (Figure 1c), equation (8) becomes

$$(h_c \pm (h_a - h_s))^2 = 2h_c h_t \tag{9}$$

where $h_a = H_a\sqrt{2}$, $h_s = H_s\sqrt{2}$, and $h_t = H_T\sqrt{2}$. In addition, because we are working with a system of particles aligned with the field, i.e., $\psi = 0°$, the anisotropy field H_K is equal to the coercive force H_C and thus $h_c = H_K\sqrt{2}$.

[15] In the absence of thermal fluctuations, i.e., $h_t = 0$ as a result of $T = 0$ K and/or $t \approx \tau_0$, the critical curves defined by equation (9) are controlled by the field and form two lines OA and OB (Figure 2a) which separate the Preisach diagram into three regions, labeled "positive" (plus), "negative" (minus), and "memory." For particles in the positive and negative regions there is no energy barrier to surmount in order to achieve the equilibrium position of the magnetic moment, thus they have only one stable orientation in which the magnetization can reside, i.e., they are "field blocked." Each particle in the memory region has two stable orientations separated by an energy barrier; the orientation in which the magnetization resides is therefore determined by the individual field and temperature "history" of the particle.

[16] For $T > 0$ K and/or $t \gg \tau_0$ (thus $h_t \neq 0$) the thermal critical curves (equation (9)), become parabolic (Figure 2b), intersecting at ($h_c = 0$, $h_s = h_a$) and ($h_c = 2h_t$, $h_s = h_a$). The thermal critical curves penetrate into the memory region (Figure 2b), splitting it into four parts. For particles in region 1, the temperature T and the observation time t have no affect, the region remains blocked and is able to retain a record of its magnetic history, i.e., particles in this region are thermally blocked. In the other three regions, i.e., 2, 3, and 4, particles are superparamagnetic, as the experimental time and temperature are now sufficient to cause unblocking. There is some propagation of the superparamagnetic regions 2, 3, and 4 into the field-blocked positive and negative areas; however, this does not contribute to the final remanence.

2.2. Randomly Orientated SW Particles

[17] For randomly orientated SW particles, when $\psi \neq 0°$, the coercive field (switching field) H_C (ψ) $\neq H_K$ and equation (2) no longer holds. For a general value of ψ it is not possible to express the energy barriers, and thus the positions of the thermal critical curves, analytically. Via interpolation, *Pfeiffer* [1990] derived a general expression with which to calculate the location of the thermal critical barriers for randomly orientated SW particles:

$$\Delta E_\pm = \frac{\mu_0 M_S V H_K}{2}\left(1 \pm \frac{H_a - H_s}{H_C(\psi)}\right)^{g(\psi)}$$

where

$$g(\psi) = 0.86 + 1.14\frac{H_C(\psi)}{H_K}$$

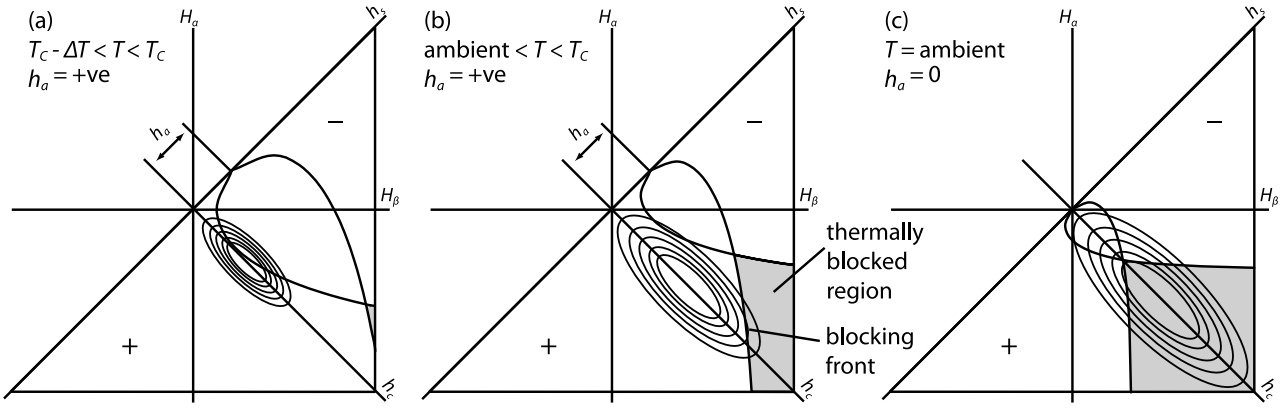

Figure 3. Schematic showing the propagation of the Preisach distribution into the Preisach plane with decreasing temperature (sequence from Figure 3a to Figure 3c) and the positions of the thermal critical barriers ($\psi = 45°$), which contract with decreasing temperature (Figure 3a then Figure 3b) and shift onto the h_c axis when the field is removed (Figure 3b then Figure 3c).

and

$$H_C(\psi) = H_K\left(\sin^{2/3}\psi + \cos^{2/3}\psi\right)^{-3/2} \tag{10}$$

Applying equation (10) to equation (9) yields

$$\frac{h_c}{2}\frac{H_K}{H_C(\psi)}\left(1 \pm \frac{h_a - h_s}{h_c}\right)^{g(\psi)} = h_t \tag{11}$$

The general shapes of the thermal critical curves for $\psi \neq 0°$ are similar to those for $\psi = 0°$ (Figure 2b). It should be noted, however, that given the dependency on the orientation the thermal critical barriers take the form of curved surfaces and only appear as lines for a single value of ψ (for example as shown in Figure 2b). For the general case there are two points of intersection: the first, ($h_c = 0$, $h_s = h_a$) and the second when $h_s = h_a$, with a corresponding value of h_c given by

$$h_c = 2h_t\frac{H_C(\psi)}{H_K}. \tag{12}$$

3. A Thermally Activated Preisach Model With Thermally Variable Distributions

[18] To simulate thermoremanence acquisition it is necessary to incorporate the strong thermal variability of the thermal critical curves (equation (11)) and the Preisach distribution $p(H_\alpha, H_\beta)$ (in Preisach space this is $p(h_c, h_s)$) into the thermally activated Preisach model described in section 2 [*Spinu et al.*, 2001; *Borcia et al.*, 2002a, 2002b].

[19] In the treatment of the thermal variability we make certain necessary assumptions: first, for the thermal critical curves, from molecular field theory for crystals greater than a few nanometers in size, $M_S(T) \propto (1 - T/T_C)^{0.5}$, where T_C is the Curie temperature [*Aharoni*, 2000]. This assumption is required because in our procedure the sample cannot be heated, and therefore $M_S(T)$ cannot be quantified experimentally. For the thermal critical curves, the variation of $H_K(T)$, is also required; as we are assuming the magnetic anisotropy is controlled by the shape anisotropy $H_K(T) \propto M_S(T)$ [*Dunlop and Özdemir*, 1997]. In Appendix A we verify this assumption that $H_K(T) \propto M_S(T)$ as a first approximation using published experimental data. Second, for the Preisach distribution $p(h_c, h_s)$ we draw on *Néel*'s [1953] interpretation of the Preisach model, where h_c corresponds to the coercive force and h_s corresponds to the interaction field; therefore $h_c(T) \propto M_S(T)$ corresponds in a similar manner to $H_K(T)$. For the variation of $h_s(T)$ we draw on the experimental findings of *Dunlop and West* [1969] and *Muxworthy and Dunlop* [2002], who both found $h_s(T) \propto M_S(T)$; that is, the interaction field is directly related to the magnetization.

[20] As illustrated in Figure 3, the critical curves and the Preisach distribution respond in the opposite sense to changes in temperature; the critical curves contract ("tightening the knot") as the temperature decreases, whereas $p(h_c, h_s)$ expands from the origin, growing outward in both the h_c and $\pm h_s$ directions. During the simulation of thermoremanence acquisition (section 4), at high temperatures approaching T_C, the distribution $p(h_c, h_s)$ is mostly in the field blocking or superparamagnetic regions (2, 3, and 4) defined by the critical curves (Figure 3a), moving gradually into the thermally blocked region 1 as the temperature decreases (Figure 3b). Finally, when the external field is reduced to zero the critical curves and memory region are centered along the h_c axis (Figure 3c).

[21] In the superparamagnetic regions the magnetic state of particles is considered to be in thermal equilibrium, with the equilibrium magnetization, M_{eq}, being given by [*Néel*, 1949]

$$M_{eq} = M_S\tanh\left(\frac{\mu_0 V M_S H}{k_B T}\right) \tag{13}$$

where H is the external field given by equation (3). On passing into the thermal blocking region 1 (the remanence carrying region), the TRM for identical particles becomes blocked (frozen) in the equilibrium state at the blocking

temperature, that is [*Stancu and Spinu*, 1998; *Roshko and Viddal*, 2004],

$$\mathrm{TRM} = M_S \tanh\left(\frac{\mu_0 V M_S(T_B)(H_a - H_s(T_B))}{k_B T_B}\right) \quad (14)$$

where T_B is the blocking temperature, $M_S(T_B)$ is the saturation magnetization at the blocking temperature, and $H_s(T_B)$ is the interaction field at the blocking temperature.

4. Using Preisach Distributions to Model Thermoremanence Acquisition for Natural Samples

4.1. First-Order Reversal Curve Diagrams as Input Preisach Distribution

[22] To simulate thermoremanence acquisition and its dependency on the external field for a real system, we require an input Preisach distribution. To do this, we employ the method of *Stoleriu and Stancu* [2006], which utilizes measured first-order reversal curve (FORC) data [*Pike et al.*, 1999; *Roberts et al.*, 2000] as the initial input. *Stoleriu and Stancu* [2006] proposed that two FORC diagrams should be measured for a given sample, one saturated in the positive magnetic field direction and the other in the negative field direction, which can then be combined by interpolation to generate a Preisach distribution. The success of this method was tested by comparing the FORC-generated Preisach distribution against a micromagnetic model [*Stoleriu and Stancu*, 2006]. It can be assumed that most rocks are magnetically isotropic, thus the method of *Stoleriu and Stancu* [2006] is identical to rotating a FORC distribution about the H_c axis at $H_s = 0$, adding the rotated FORC distribution to the original FORC distribution and dividing by two (see Appendix B for more details).

[23] To reduce the effects of measurement noise, the FORC distribution is determined at each point by piecewise fitting of a second-order polynomial trend surface to the measured data [*Muxworthy and Roberts*, 2007]. The span of the local area is determined by a user-defined smoothing factor (SF), which is usually between 2 and 5. The resultant shape of the FORC distribution, and the input Preisach distribution, thus depends on the choice of SF. In Appendix B, we outline an approach of estimating the FORC distribution for SF = 0, which we use as the input for our Preisach distribution.

4.2. Modeling of Thermoremanence Acquisition for Natural Samples

[24] To simulate thermoremanence (TRM) acquisition numerically, we generate $\sim 2 \times 10^6$ hysterons whose properties were controlled by the input Preisach distribution, i.e., each hysteron is assigned values of h_c and h_s picked using the Preisach distribution as an empirical probability density function (thus, we are not required to approximate the Preisach distribution with preselected basis functions). With this statistical approach we do not try to accurately predict the behavior of individual magnetic crystals, but of an assemblage as a whole. During simulated TRM acquisition or other magnetic processes, the history of each hysteron and its corresponding magnetization state is recorded. Magnetization states can change on moving across energy barrier fronts. Summation of the hysterons gives the net magnetization. The number of hysterons generated is far greater than is needed during Preisach simulation of say isothermal remanence acquisition [e.g., *Heslop et al.*, 2004], because the proportion contributing to the net thermoremanence is relatively smaller.

[25] The position of the thermal critical barriers for each hysteron depends on three related variables ψ, V and H_K (equations (10) and (11)). Each hysteron is assigned an angle ψ drawn randomly from a uniform distribution on the surface of a unit sphere; however, there is no unique solution to the determination of V and H_K required in the model simulation. To resolve this we turn to an empirical relationship first described by *Barbier* [1954], which relates the thermal fluctuation field H_f to the experimentally determined coercive force H_C. The thermal fluctuation field was defined for aligned particles by *Wohlfarth* [1984] as

$$H_f = \frac{k_B T}{\mu_0 M_S V_{act}} \quad (15)$$

where V_{act} is the activation volume. It is often assumed that V_{act} is identical to the actual volume for isolated "ideal" single-domain (SD) grains, and for multidomain (MD) grains the effective volume covered by a single jump between pinning sites for a domain wall or other such domain wall events [*Wohlfarth*, 1984]. For SD grains thought to switch via coherent rotation, this assumption appears to be correct in the case of magnetite and thus magnetic granulometry techniques can be based on the determination of V_{act} [*Dunlop*, 1976]. Studies on interacting particles, however, have shown that the estimated V_{act}, is greater than the volume of individual magnetic particles [e.g., *El-Hilo and Bsoul*, 2007].

[26] Our thermoremanence model is based on the behavior of SW particles that exhibit coherent rotation, therefore, $V \approx V_{act}$ and H_T given in equation (8), can be written as

$$H_T = H_f \ln\left(\frac{t}{\tau_0}\right) \quad (16)$$

There are numerous experimental methods with which to determine H_f. For example, measurement of the time dependency of remanent or induced magnetization, e.g., viscous decay curves [*Sholpo*, 1967], or by determining the time dependency of hysteresis, e.g., variable field sweep rate hysteresis [*Bruno et al.*, 1990; *Muxworthy et al.*, 2009].

[27] The empirical relationship between H_f and H_C first reported by *Barbier* [1954] was later refined by *Wohlfarth* [1984], who found that $H_C \propto V_{act}^{-0.73}$ for a wide range of materials covering several orders of magnitude of H_C. *Wohlfarth* [1984] did not, however, consider any natural materials in his study, and thus, *Muxworthy et al.* [2009] tested this relationship for a series of basaltic lavas from various locations, obtaining $H_C \propto V_{act}^{-0.68}$, which, as shown by *Muxworthy et al.* [2009], leads to $H_f \propto H_C^{0.54}$. *Muxworthy et al.* [2009] suggest four possible reasons for this difference, the most important being that the original fit to the Barbier data essentially examines behavioral trends between a wide range of different materials, whereas, although the basalts examined have a variety of compositions, they are essentially the "same" material, i.e., titanomagnetites with

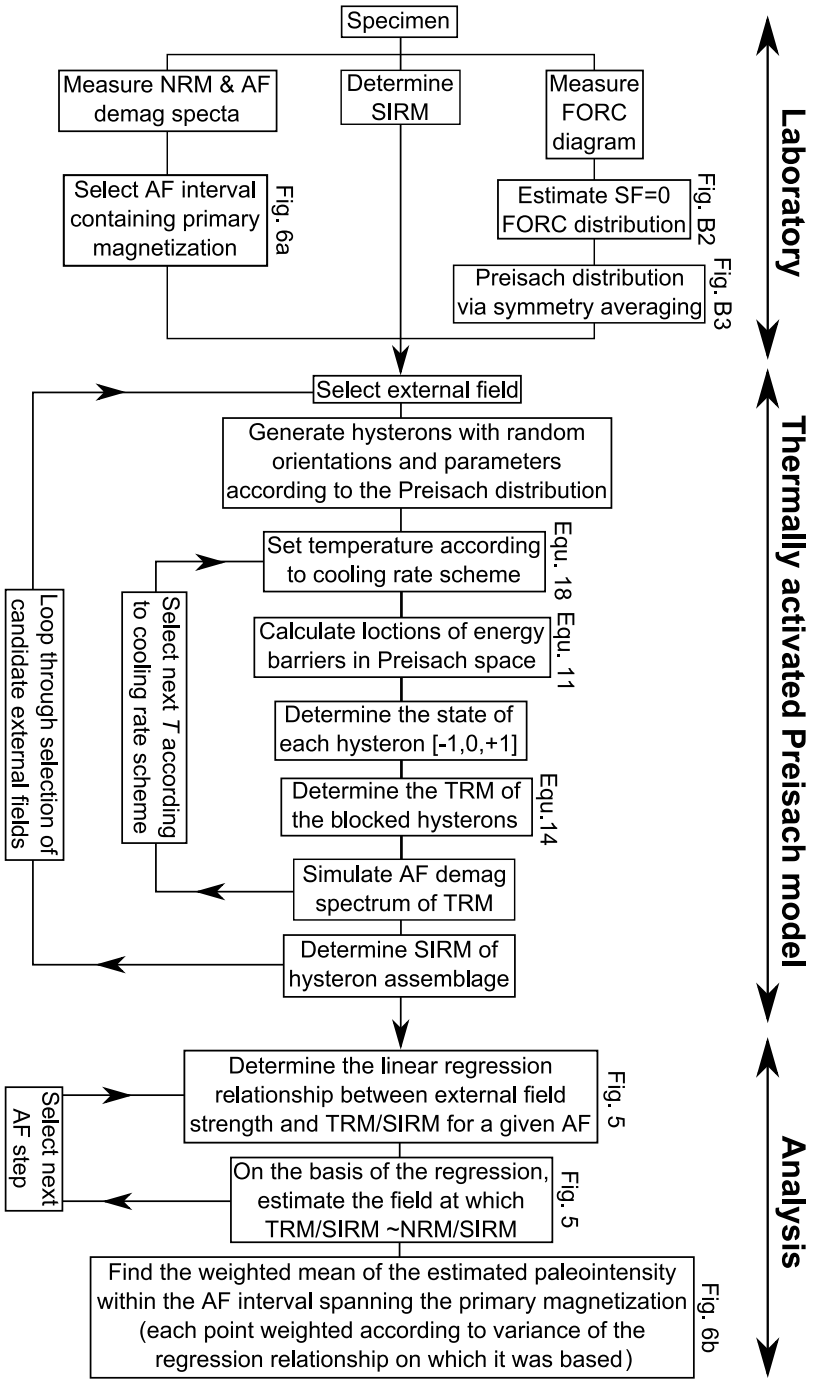

Figure 4. A flow diagram detailing the measurement requirements, numerical algorithm and procedure for making absolute paleointensity estimates using the Preisach method.

varying degrees of oxidation. Using the relationship reported by *Muxworthy et al.* [2009], equation (16) can be rewritten as

$$H_T = \frac{H_C^{0.54}}{10^{0.52}} \ln\left(\frac{t}{\tau_0}\right) \tag{17}$$

where H_C is the empirically determined coercive force, i.e., h_c in the Preisach distribution ($H_C = h_c/\sqrt{2}$). Using this empirical relationship means that we no longer require V, allowing us to determine H_K using equations (10), (11) and (17) for a randomly drawn angle ψ. There is no analytical solution to the calculation of H_K; however, it is straightforward to numerically determine the root [*Press et al.*, 1992] and hence to obtain H_K for each hysteron. A sensitivity study of equation (17) is conducted by *Muxworthy et al.* [2011].

[28] In the model for thermoremanence acquisition we determine the state and history of each hysteron during simulated cooling in an applied field. The cooling is

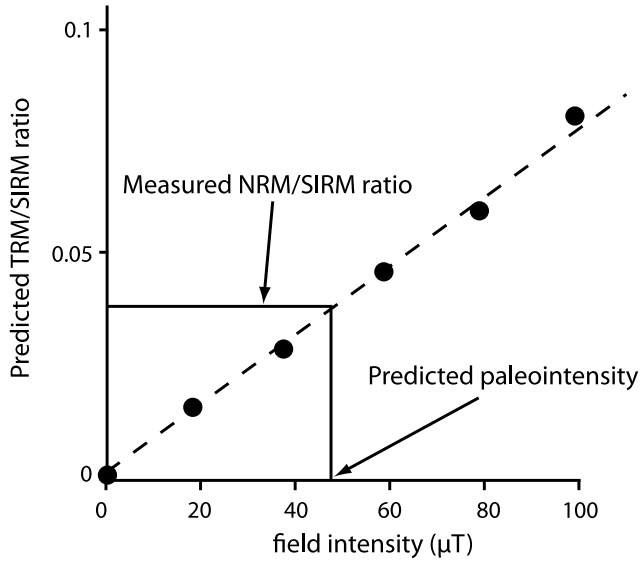

Figure 5. Schematic to demonstrate how the paleointensity is estimated. For a given input Preisach distribution the model predicts the ratio of TRM/SIRM versus field intensity. To assess the numerical consistency within the model calculation, the Preisach distribution, constructed from 2×10^6 randomly orientated hysterons, is resampled for each field simulation, i.e., constructed using a total of 12×10^6 hysterons. The paleointensity is estimated by comparing the measured NRM/SIRM ratio with the linear fit. The plot is from data for a sample from the 1944 eruption of Paricutin, Mexico, where the field was 45 μT. See *Muxworthy et al.* [2011] for further details. A total cooling time of 1 month was assumed for the lava (equation (19)).

discretized, i.e., the temperature is changed in a series of small increments and the position of the hysterons relative to the thermal critical curves is calculated for each step. The position of the thermal critical curves depends on the time t, however, as the temperature is constantly changing, $t \approx 0$ for any single temperature. Previous studies [e.g., *Dodson and McClelland-Brown*, 1980; *Halgedahl et al.*, 1980] have circumnavigated this problem by taking discrete time intervals, i.e., an equivalent time, t_{eq}, determined by the cooling rate, i.e., $t_{eq} = \Delta T/(\partial T/\partial t)$, where typically $\Delta T = 1$ K. In our simulated TRM expression we use a more rigorous expression for t_{eq} (=t) obtained by numerically solving the master equation [*Spinu et al.*, 2001; *Borcia et al.*, 2002a], i.e.,

$$t_{eq} = \frac{H_a T}{H_f\left(\frac{\partial T}{\partial t}\right)} \tag{18}$$

where $\partial T/\partial t$ is the rate of change of temperature with time, i.e., the cooling rate. Equation (18) effectively increases t_{eq} by the absolute temperature compared to the discretized approach, as $H_a \approx H_f$. This underestimation in the discretized approximation is due to making a linear approximation of a nonlinear system.

[29] For $\partial T/\partial t$ we have employed the standard Newtonian cooling rate equation:

$$T - T_R = (T_C - T_R)e^{-t/A} \tag{19}$$

where T_R is the final temperature and A is a constant determined by considering how long it takes to cool from T_C to within 1% of T_R [*Halgedahl et al.*, 1980], i.e., A = (total time)/ln[$(0.01 \times T_R)/(T_C - T_R)$].

4.3. Protocol for Estimating a Paleointensity From a Natural Sample

[30] Using the described model, it is possible to make a TRM intensity estimate for a given FORC distribution as a function of applied field and cooling rate. However, further information is required from the sample in order to estimate paleointensity, primarily the natural remanent magnetization (NRM), necessarily determined before the FORC distribution is measured, and the saturation isothermal remanence (SIRM). The NRM is required as this contains the original paleomagnetic information, and the SIRM to normalize both the experimental NRM and the predicted TRM. It is routine to predict the SIRM intensity of a Preisach distribution [*Bertotti*, 1998]. A flowchart detailing the measurement procedure and paleointensity estimation algorithm is shown in Figure 4.

[31] For a recent lava sample the recorded field intensity can simply be estimated by comparing the measured NRM/SIRM ratio with the predicted TRM/SIRM ratios determined as a function of field intensity (Figure 5); however, in older geological samples it is unlikely that the NRM is a single-component TRM. Often samples have acquired an overprint magnetization due to secondary heating or the acquisition of viscous magnetization, thus it is necessary to alternating field (AF) demagnetize the NRM in order to identify secondary magnetizations. The AF demagnetization data (Figure 6) is then plotted on orthogonal projection plots [*Zijderveld*, 1967] and primary and secondary magnetizations identified visually (Figure 6a). Because the sample NRM is AF demagnetized, we must similarly simulate AF demagnetization in the Preisach model (Figure 6a), which is straightforward [*Dunlop and Özdemir*, 1997]. This simulation of the measured AF demagnetization curve acts as an internal consistency check; data points with large deviations between the predicted and actual magnetizations are not used in the determination of the paleointensity, where large deviations maybe due to the presence of chemical remanent magnetization. Animation S1, showing the simulation of thermoremanence acquisition and subsequent AF demagnetization for a sample from Iceland, is provided in the auxiliary material.[1]

[32] As the primary magnetization (Figure 6a) is defined over a series of AF demagnetization steps, rather than make a single paleointensity estimation it is possible to make an estimation for each AF demagnetization field associated with the primary magnetization (Figure 6). This approach is similar in "spirit" to that in the REM's relative paleointensity method [*Gattacceca and Rochette*, 2004].

[33] In both the experimental data and the Preisach simulation, as the AF demagnetization reduces the magnetization toward zero the robustness of the estimate decreases (Figure 6b). To account for this we introduce two criteria: first, we reject data for AF demagnetization steps where the

[1] Auxiliary materials are available in the HTML. doi:10.1029/2010JB007843.

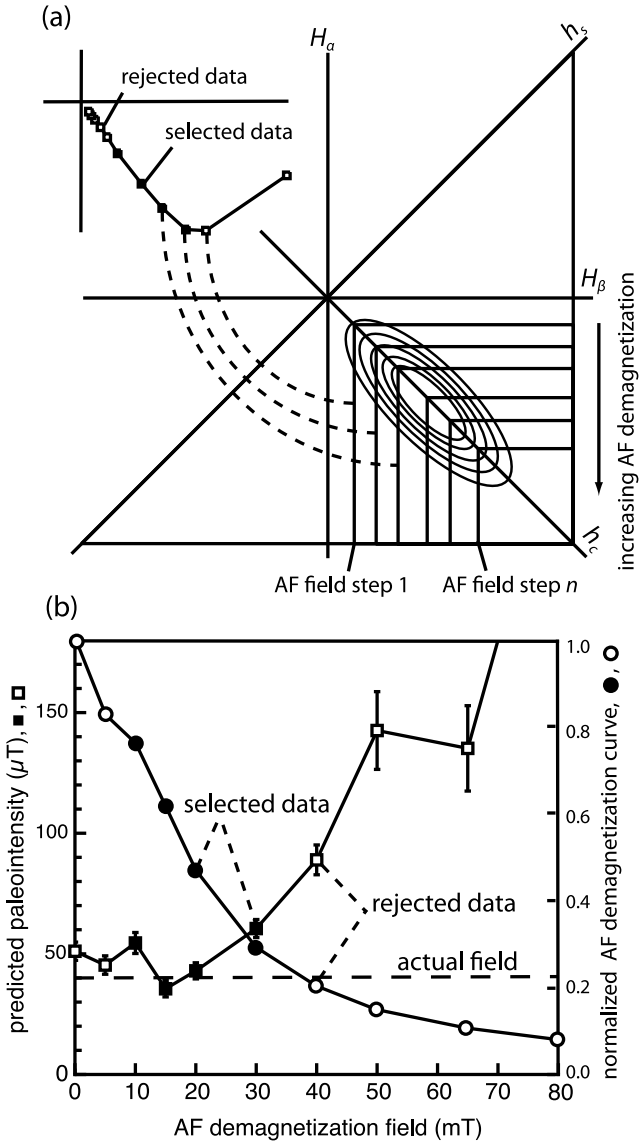

Figure 6. (a) Schematic of simulated AF demagnetization in the Preisach plane with the inset showing an orthogonal projection ("Zijderveld") plot for the AF demagnetization data for a Mexican lava sample shown in Figure 6b. For paleointensity analysis, only part of the magnetization is selected from the orthogonal projection, i.e., the segment identified with the primary magnetization of the sample. (b) AF demagnetization data for a lava sample from the 1944 eruption of Paricutin, Mexico, where the field was 45 μT (see *Muxworthy et al.* [2011] for further details), and predicted paleointensity estimates for each AF demagnetization step. Only steps associated with the primary magnetization are selected (solid). Points where the normalized AF demagnetization is <0.2 are also rejected as they were found to be strongly susceptible to noise. A total cooling time for the lava of 1 month was assumed (equation (19)).

magnetization is <20% its original value, i.e., NRM(AF)/NRM(original) <0.2. Second, we make an average prediction of the paleointensity, inversely weighted by the variances of the fitted linear regression models (Figure 5) for the selected AF steps. Generally as NRM(AF demagnetized)/NRM(original) $\rightarrow$ 0.2, the variance increases, making the exact position of the cutoff in the weighted average noncritical. However, a cutoff value is still required, as very low values of NRM(AF demagnetized)/NRM(original) are often associated with noise and can yield highly erratic paleointensity estimates (Figure 6b).

5. Limitations of the Model

[34] *Muxworthy et al.* [2011] report an empirical test of the new protocol. However, before examining the data, there are a number of theoretical considerations, which we address here.

5.1. Natural Remanent Magnetizations That Are Not of a Thermoremanent Origin

[35] In the model we assume that the NRM is a TRM in origin. As we do not have robust physical models for the alternative class of possible remanent magnetizations, i.e., chemical remanent magnetization (CRM) including thermochemical remanent magnetizations (TCRM), we have no choice at present but to limit the approach to TRM. All existing absolute paleointensity methods, e.g., the Thellier method, which stepwise replaces the NRM with a laboratory TRM, make the same assumption and although there are checks within the protocol that attempt to identify TCRM and CRM it is well known that these checks are not definitive. Discriminating between TRM, CRM and TCRM remains a challenging task.

[36] The Preisach model compares simulated and measured AF demagnetization curves, and rejects data points with large deviations between these curves. It is suggested that large deviations maybe due to the presence of CRM or TCRM components.

5.2. Do FORC Distributions Represent a True Probability Distribution?

[37] We have effectively used the FORC distribution as a probability distribution; however, it has been shown both theoretically [*Muxworthy et al.*, 2004; *Newell*, 2005] and experimentally [e.g., *Carvallo et al.*, 2004] that FORC distributions can display negative regions. This is potentially a serious flaw; however, negative contributions to the FORC distribution only occur in the field-blocked regions (labeled positive and negative in Figure 2a) and do not contribute to the net remanence. Therefore, negative contributions to the FORC distribution are only an issue if FORC generated Preisach diagrams are to be used to model in-field measurements. This is one of the reasons that we choose to normalize the TRM intensity by the SIRM, and not the saturation magnetization (section 4.3). Therefore, while our input Preisach distribution may not be a true probability distribution over the entire Preisach space, within the region of interest, i.e., the memory region (Figure 2a), it can be treated as such.

5.3. Non-SW Behavior and the Preisach Paleointensity Method

[38] The theoretical framework for the Preisach paleointensity protocol is based on interacting SW particles. This is an advance on previous paleointensity protocols, as it is

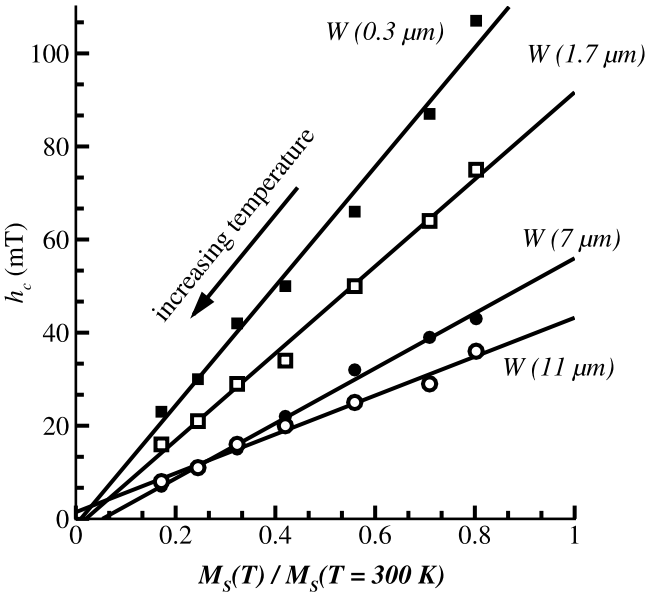

Figure A1. Variation of coercive force as identified from FORC diagrams versus the variation in saturation magnetization for four synthetic sized magnetite samples: W (0.3 μm), W (1.7 μm), W (7 μm), and W (11 μm). The data were originally collected by *Muxworthy and Dunlop* [2002] and are reanalyzed here.

the first method that actively includes interactions in its theoretical framework (it should be noted that some paleointensity methods have an empirical basis, thus making no assumptions concerning interactions [e.g., *Dekkers and Böhnel*, 2006]).

[39] Non-SW behavior can be split broadly into two: (1) unstable or nonremanence carrying, i.e., multidomain behavior, and (2) stable or remanence carrying, i.e., essentially pseudosingle-domain (PSD) behavior. Generally speaking, "true" MD behavior contributes to the field-blocked regions of the FORC distribution labeled positive and negative in Figure 2a [*Pike et al.*, 2001]. As discussed in section 5.2, the Preisach distribution in these regions does not contribute to the remanence, and therefore does not influence the predicted paleointensity.

[40] PSD behavior appears to contribute to all three regions; positive, negative, and memory in Figure 2a [*Muxworthy and Dunlop*, 2002]. As there is no robust theoretical or numerical model for PSD thermoremanence acquisition, it is difficult to define exactly how PSD TRM should be represented in Preisach space. The positions of the thermal critical barriers (equation (11)), are based on Boltzmann statistics for randomly orientated SW particles, i.e., systems with a choice between two minima. In PSD grains the number of possible stable states is likely to be higher [*Rave et al.*, 1998], making the application of Boltzmann statistics for a two state system incorrect. However, we argue that it serves as a first-order approximation, and in some cases equation (11) may be appropriate for PSD grains, for example, in small PSD grains with simple vortex structures, the center or core of the vortex is thought to be the main remanence carrier, and for an elongated grain this may have only two favorable orientations, i.e., similar to a SW particle.

[41] We propose that the model better accommodates non-SW behavior in two additional ways. First, by the inclusion of interactions through the spread in the h_s axis (Figure 1c); until now we have discussed these interactions as intergrain interactions between SD grains, but they can also represent interdomain interactions within a PSD or MD grain. Second, for PSD and MD grains the activation volume V_{act} (equation (13)), is not identical to the actual particle volume but is associated with volume covered by a domain wall movement [*Wohlfarth*, 1984]. Therefore, even though the model is for SW particles, there are many parts of the model that also apply to non-SW grains.

[42] It is also possible for SD grains to have higher-order anisotropy, e.g., cubic anisotropy, increasing the number of

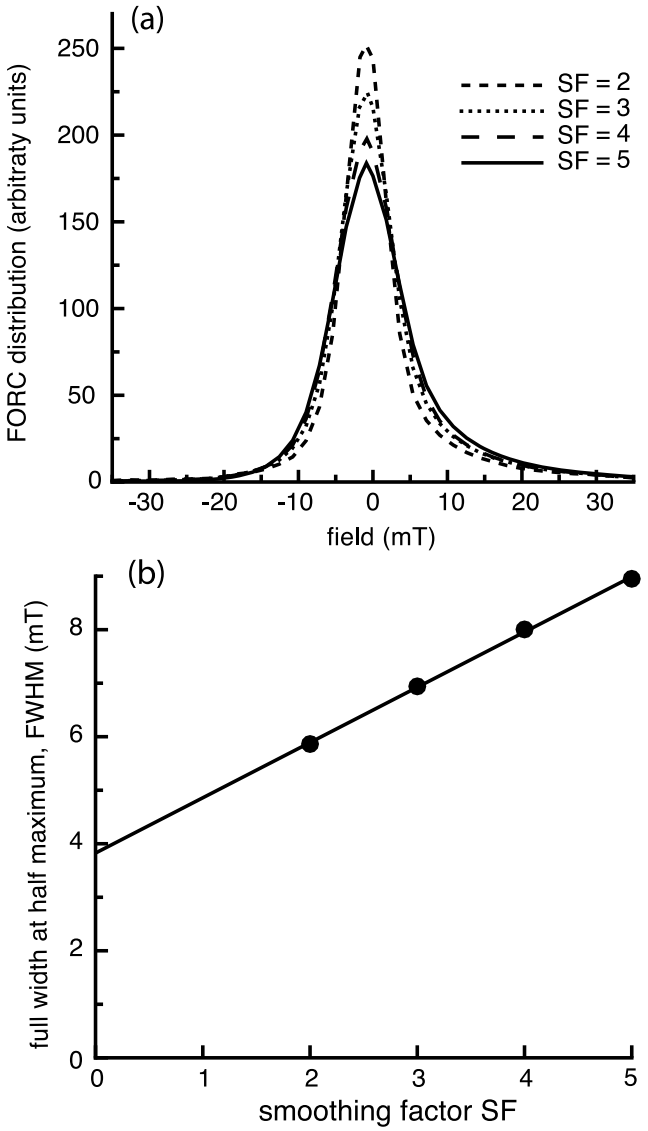

Figure B1. (a) Vertical profiles of the FORC distribution through the peak of the distribution for four smoothing factors. Such profiles are used to determine the full width at half maximum (FWHM) parameter. The data are from a lava sample from the 1944 eruption of Paricutin, Mexico (sample P1BX). (b) FWHM versus smoothing factor for the data shown in Figure B1a, with a linear extrapolation for SF = 0.

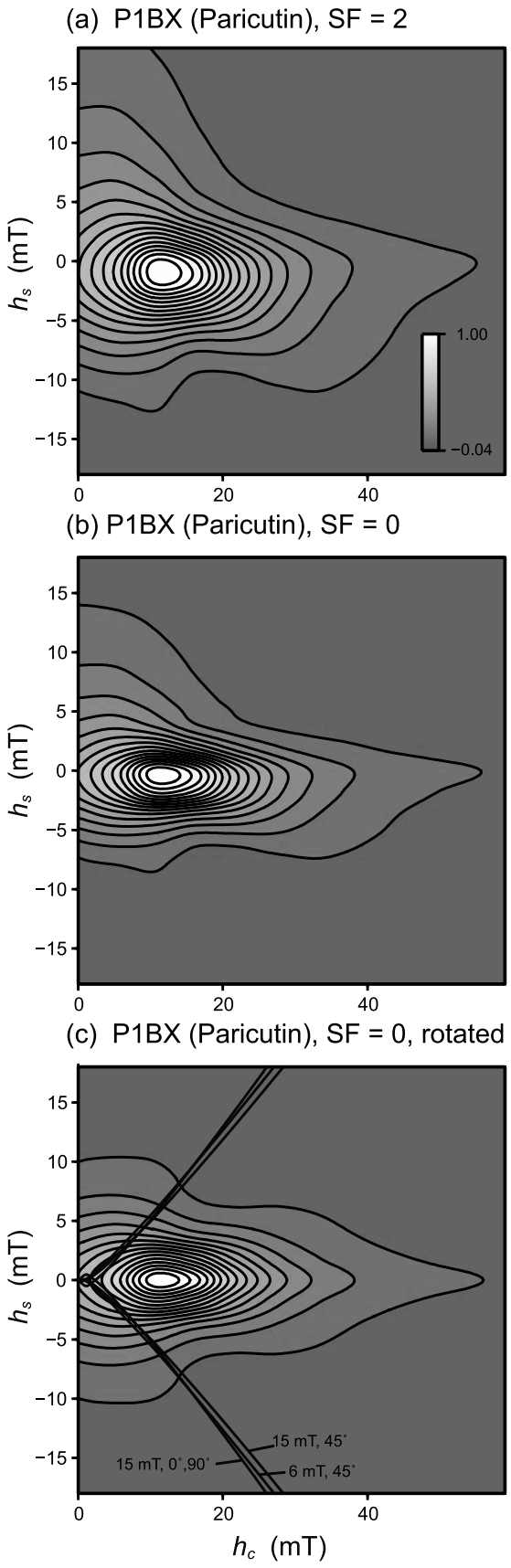

possible states [*Newell*, 2006] in a similar fashion to PSD grains. The actual effective anisotropy is hard to predict due to the importance of shape; however, for (magnetite) grains with an extension of only 1.15–1.2, the shape starts to dominate the anisotropy. Surface roughness also increases the uniaxial behavior of small grains [*Williams et al.*, 2010]. There are very few reports in the geophysical literature of reduced magnetization ratios >0.5 [*Kneller*, 1969], suggesting that SD grains with higher-order anisotropy are rare in nature [*Fabian*, 2006].

6. Conclusions

[43] In this paper a new nonheating protocol for estimating absolute paleointensities is described for rocks whose primary remanence is a TRM. Because we have removed the requirement for heating from the experimental protocol, chemical alteration in the laboratory can be avoided making it possible to investigate a wide range of materials not suitable for traditional Thellier-type experiments.

[44] The proposed method is based on a thermally activated Preisach model with thermal variance included. This is the first paleointensity protocol that includes magnetic interactions within its theory, and accommodates, on a first-order approximation, non-SD behavior, e.g., true MD behavior does not affect the final paleointensity estimate. The Preisach distribution for a given sample is obtained from a FORC distribution measurement, and the paleointensity is estimated by comparison to the AF demagnetization of the NRM. Depending on laboratory facilities, the total measurement time should be substantially less than that required to make a Thellier-type paleointensity estimation, though we see this method as being applicable only when Thellier-type methods are inappropriate, for specimens such as meteoritic samples that are thermally unstable. Compared to other nonheating methods, e.g., the REM family of methods, the new protocol will be generally slower, but more accurate as is demonstrated in the following paper. Rigorous testing of the new nonheating protocol is reported by *Muxworthy et al.* [2011].

Appendix A: Thermal Dependency of $h_c(T)$

[45] In the model the thermal dependency of $h_c(T)$ is required, where $h_c(T)$ is the coercive force for an individual

Figure B2. (a) A FORC diagram for SF = 2 for the lava sample from the 1944 eruption of Paricutin (sample P1BX), Mexico, shown in Figure A1. (b) The same FORC distribution as in Figure B2a but extrapolated in the h_s direction for SF = 0. This procedure is performed before the FORC diagram is rotated and averaged to produce a symmetrical Preisach distribution (c). Representative energy barriers are drawn on the symmetrical Preisach distribution for selected conditions. The energy barriers given by equation (9) are different for every hysteron and depend on the hysteron's coercive force and the hysteron's angle relative to the applied field as well as the temperature and the measurement time. For comparison with the room temperature data, three barriers are drawn for three hysterons for a measurement time of 0.1 s at 300 K.

hysteron or group of similar hysterons. As the model is based on Stoner-Wohlfarth particles, $h_c(T) \propto M_S(T)$. In this appendix we verify this relationship experimentally, by considering the high-temperature FORC data of *Muxworthy and Dunlop* [2002]. *Muxworthy and Dunlop* [2002] measured FORC distributions between room temperature and the Curie temperature, for four sized synthetic magnetite samples: W (0.3 μm), W (1.7 μm), W (7 μm), and W (11 μm), where the arithmetic mean grain size is in the sample name.

[46] *Muxworthy and Dunlop* [2002] determined and plotted the bulk coercive force $H_c(T)$ as a function of temperature. This did not vary as $M_S(T)$, but it is important to note that $H_c(T) \neq h_c(T)$. As temperature increases, $H_c(T)$ is a measure of both the real decrease in each individual particle's coercive force plus the contribution from thermally relaxed systems. To determine the thermal behavior of $h_c(T)$ key features of the FORC diagram on the h_c axis were indentified, e.g., a consistent "kink" in the FORC distribution, and examined how these features evolved with temperature. For each sample, a feature was identified at each temperature and its h_c value plotted versus the reduced spontaneous magnetization (Figure A1). A linear trend is fitted to the data for each sample. As a first approximation it is seen that $h_c(T) \propto M_S(T)$.

Appendix B: Estimation of the FORC Distribution for SF = 0

[47] The determination of a FORC distribution involves the estimation of a mixed second derivative by piecewise fitting of second-order trend surfaces [*Roberts et al.*, 2000]. The size of the local area to which a surface is fitted is controlled by a user-defined smoothing factor (SF, expressed in terms of a number of data points), where the total size of the grid is $(2SF+1)^2$. SF normally takes values between 2 and 5, although where possible it should be 2 in order to avoid excessive smoothing of the data. Increasing SF reduces the contribution of measurement noise to the resulting FORC diagram, but it will also distort the underlying FORC distribution. Simple tests can be conducted to determine suitable smoothing factors for each sample [*Heslop and Muxworthy*, 2005; *Harrison and Feinberg*, 2008].

[48] The control of SF on the shape of the FORC distribution can be illustrated by considering the full width at half maximum (FWHM) of the profile in the vertical ("interaction field") direction through the FORC distribution peak [*Muxworthy and Dunlop*, 2002]. As SF increases, the absolute width of the FORC distribution profile does not increase significantly (Figure B1a); however, as the peak value decreases, FWHM decreases (Figure B1b).

[49] Ideally, the effect of SF should be removed from the input-Preisach distribution. When using the piecewise fitting approach to determine the mixed second derivative, setting SF = 0 is not possible. In our Preisach paleointensity protocol, we use a simple approximation for SF = 0. After examination of several hundred FORC distributions [*Muxworthy et al.*, 2011], we observed that (in all but two or three cases) FORC distributions displayed a linear relationship between SF and FWHM (Figure B1b). As an approximation for SF = 0, we take a linear extrapolation determined over $2 \leq SF \leq 5$, for SF = 0, and adjust the FORC distribution in the vertical direction (Figure B2). For completeness the sample is also rotated and averaged to form the input Preisach distribution.

[50] In Figure B2c representative energy barriers are drawn using equation (9) for three representative hysterons; each hysteron experiences its own energy barriers, as the position of the barriers depends on the hysteron's coercive force and angle relative to the applied field as well as the temperature and the measurement time.

[51] **Acknowledgments.** This work was funded by NERC grant NE/D000351/1, by the Royal Society, and through DFG-Research Center/Cluster of Excellence "The Ocean in the Earth System." The FORTRAN 95 source code to perform the outlined paleointensity estimations is available on request from the authors.

References

Aharoni, A. (2000), *Introduction to the Theory of Ferromagnetism*, 2nd ed., 319 pp., Oxford Univ. Press, Oxford, U. K.

Barbier, J. C. (1954), Le traînage magnétique de fluctuation, *Ann. Phys.*, *9*, 84–140.

Bertotti, G. (1998), *Hysteresis in Magnetism*, 558 pp., Academic, San Diego, Calif.

Borcia, I. D., L. Spinu, and A. Stancu (2002a), A Preisach-Néel model with thermally variable variance, *IEEE Trans. Magn.*, *38*(5), 2415–2417, doi:10.1109/TMAG.2002.803611.

Borcia, I. D., L. Spinu, and A. Stancu (2002b), Simulation of magnetization curves with Preisach-Neel models, *J. Magn. Magn. Mater.*, *242–245*, 1034–1037, doi:10.1016/S0304-8853(01)01127-1.

Bruno, P., G. Bayreuther, P. Beauvillain, C. Chappert, G. Lugert, D. Renard, J. P. Renard, and J. Seiden (1990), Hysteresis properties of ultrathin ferromagnetic films, *J. Appl. Phys.*, *68*(11), 5759–5766, doi:10.1063/1.346944.

Carvallo, C., Ö. Özdemir, and D. J. Dunlop (2004), First-order reversal curve (FORC) diagrams of elongated single-domain grains at high and low temperatures, *J. Geophys. Res.*, *109*, B04105, doi:10.1029/2003JB002539.

Coe, R. S. (1967), The determination of paleointensities of the Earth's magnetic field with emphasis on mechanisms which could cause non-ideal behavior in Thellier's method, *J. Geomagn. Geoelectr.*, *19*, 157–179.

Dekkers, M. J., and H. N. Böhnel (2006), Reliable absolute palaeointensities independent of magnetic domain state, *Earth Planet. Sci. Lett.*, *248*(1–2), 508–517.

Dodson, M. H., and E. McClelland-Brown (1980), Magnetic blocking temperatures of single-domain grains during slow cooling, *J. Geophys. Res.*, *85*(B5), 2625–2637, doi:10.1029/JB085iB05p02625.

Dunlop, D. J. (1976), Thermal fluctuation analysis: A new technique in rock magnetism, *J. Geophys. Res.*, *81*, 3511–3517, doi:10.1029/JB081i020p03511.

Dunlop, D. J. (1998), Thermoremanent magnetization of nonuniformly magnetized grains, *J. Geophys. Res.*, *103*(B12), 30,561–30,574, doi:10.1029/98JB00026.

Dunlop, D. J., and Ö. Özdemir (1997), *Rock Magnetism: Fundamentals and Frontiers*, 573 pp., Cambridge Univ. Press, Cambridge, U. K., doi:10.1017/CBO9780511612794.

Dunlop, D. J., and G. F. West (1969), An experimental evaluation of single-domain theories, *Rev. Geophys.*, *7*, 709–757, doi:10.1029/RG007i004p00709.

Dunlop, D. J., B. X. Zhang, and O. Ozdemir (2005), Linear and nonlinear Thellier paleointensity behavior of natural minerals, *J. Geophys. Res.*, *110*, B01103, doi:10.1029/2004JB003095.

El-Hilo, M., and I. Bsoul (2007), Interaction effects on the coercivity and fluctuation field in granular powder magnetic systems, *Physica B*, *389*, 316–326, doi:10.1016/j.physb.2006.07.003.

Fabian, K. (2001), A theoretical treatment of paleointensity determination experiments on rocks containing pseudo-single or multi domain magnetic particles, *Earth Planet. Sci. Lett.*, *188*(1–2), 45–58, doi:10.1016/S0012-821X(01)00313-2.

Fabian, K. (2006), Approach to saturation analysis of hysteresis measurements in rock magnetism and evidence for stress dominated magnetic anisotropy in young mid-ocean ridge basalt, *Phys. Earth Planet. Inter.*, *154*(3–4), 299–307, doi:10.1016/j.pepi.2005.06.016.

Folgerhaiter, G. (1899), Sur les variations séculaires de l'inclinaison magnétique dans l'antiquité, *J. Phys.*, *8*, 660–667.

Fuller, M., S. Cisowski, M. Hart, R. Haston, and E. Schmidtke (1988), NRM:IRM(s) demagnetization plots: An aid to the interpretation of

natural remanent magnetization, *Geophys. Res. Lett.*, *15*, 518–521, doi:10.1029/GL015i005p00518.
Gattacceca, J., and P. Rochette (2004), Toward a robust normalized magnetic paleointensity method applied to meteorites, *Earth Planet. Sci. Lett.*, *227*(3–4), 377–393, doi:10.1016/j.epsl.2004.09.013.
Halgedahl, S. L., R. Day, and M. Fuller (1980), The effect of cooling rate on the intensity of weak-field TRM in single-domain magnetite, *J. Geophys. Res.*, *85*(B7), 3690–3698, doi:10.1029/JB085iB07p03690.
Harrison, R., and J. M. Feinberg (2008), FORCinel: An improved algorithm for calculating first-order reversal curve distributions using locally weighted regression smoothing, *Geochem. Geophys. Geosyst.*, *9*, Q05016, doi:10.1029/2008GC001987.
Heslop, D., and A. R. Muxworthy (2005), Aspects of calculating first-order-reversal-curve distributions, *J. Magn. Magn. Mater.*, *288*, 155–167, doi:10.1016/j.jmmm.2004.09.002.
Heslop, D., G. McIntosh, and M. J. Dekkers (2004), Using time- and temperature-dependent Preisach models to investigate the limitations of modelling isothermal remanent magnetization acquisition curves with cumulative log Gaussian functions, *Geophys. J. Int.*, *157*(1), 55–63, doi:10.1111/j.1365-246X.2004.02155.x.
Kletetschka, G., P. J. Wasilewski, and P. T. Taylor (2000), Unique thermoremanent magnetization of multidomain sized hematite: Implications for magnetic anomalies, *Earth Planet. Sci. Lett.*, *176*(3–4), 469–479, doi:10.1016/S0012-821X(00)00016-9.
Kneller, E. (1969), Fine particle theory, in *Magnetism and Metallurgy*, edited by A. Berkowitz and E. Kneller, pp. 366–472, Academic, San Diego, Calif.
Koenigsberger, J. G. (1938a), Natural residual magnetism of eruptive rocks - part 1, *Terr. Magn. Atmos. Electr.*, *43*, 119–130, doi:10.1029/TE043i002p00119.
Koenigsberger, J. G. (1938b), Natural residual magnetism of eruptive rocks - part 2, *Terr. Magn. Atmos. Electr.*, *43*, 299–320, doi:10.1029/TE043i003p00299.
Levi, S. (1977), The effect of magnetite particle size on paleointensity determinations of the geomagnetic field, *Phys. Earth Planet. Inter.*, *13*, 245–259, doi:10.1016/0031-9201(77)90107-8.
Mayergoyz, I. D. (2006), Vector Preisach models of hysteresis, in *The Science of Hysteresis*, edited by G. Bertotti and I. D. Mayergoyz, pp. 447–528, Academic, Oxford, doi:10.1016/B978-012480874-4/50007-5.
Muxworthy, A. R., and D. J. Dunlop (2002), First-order reversal curve (FORC) diagrams for pseudo-single-domain magnetites at high temperature, *Earth Planet. Sci. Lett.*, *203*(1), 369–382, doi:10.1016/S0012-821X(02)00880-4.
Muxworthy, A. R., and A. P. Roberts (2007), First-order reversal curve (FORC) diagrams, in *Encyclopedia of Geomagnetism and Paleomagnetism*, edited by E. Herrero-Bervera and D. Gubbins, pp. 266–272, Springer, Dordrecht, Netherlands, doi:10.1007/978-1-4020-4423-6_99.
Muxworthy, A. R., D. Heslop, and W. Williams (2004), Influence of magnetostatic interactions on first-order-reversal-curve (FORC) diagrams: A micromagnetic approach, *Geophys. J. Int.*, *158*, 888–897, doi:10.1111/j.1365-246X.2004.02358.x.
Muxworthy, A. R., D. Heslop, and D. Michalk (2009), Thermal fluctuation fields in basalts and the Barbier plot, *Earth Planets Space*, *61*, 111–117.
Muxworthy, A. R., D. Heslop, G. A. Paterson, and D. Michalk (2011), A Preisach method for estimating absolute paleofield intensity under the constraint of using only isothermal measurements: 2. Experimental testing, *J. Geophys. Res.*, *116*, B04103, doi:10.1029/2010JB007844.
Néel, L. (1949), Théorie du traînage magnétique des ferromagnétiques en grains fins avec applications aux terres cuites, *Ann. Geophys.*, *5*, 99–136.
Néel, L. (1953), Remarques sur la théorie des propriétés magnétiques des substances dures, *Appl. Sci. Res.*, *4*, 13–24, doi:10.1007/BF02316465.
Newell, A. J. (2005), A high-precision model of first-order reversal curve (FORC) functions for single-domain ferromagnets with uniaxial anisotropy, *Geochem. Geophys. Geosyst.*, *6*, Q05010, doi:10.1029/2004GC000877.
Newell, A. J. (2006), Superparamagnetic relaxation times for mixed anisotropy and high energy barriers with intermediate to high damping: 1. Uniaxial axis in a ⟨001⟩ direction, *Geochem. Geophys. Geosyst.*, *7*, Q03016, doi:10.1029/2005GC001146.
Paterson, G. A., A. R. Muxworthy, A. P. Roberts, and C. Mac Niocaill (2010), Assessment of the usefulness of lithic clasts from pyroclastic deposits for paleointensity determination, *J. Geophys. Res.*, *115*, B03104, doi:10.1029/2009JB006475.
Pfeiffer, H. (1990), Determination of anisotropy field distribution in particle assemblies taking into account thermal fluctuations, *Phys. Status Solidi*, *118*(1), 295–306(a), doi:10.1002/pssa.2211180133.
Pike, C. R., A. P. Roberts, and K. L. Verosub (1999), Characterizing interactions in fine magnetic particle systems using first order reversal curves, *J. Appl. Phys.*, *85*(9), 6660–6667, doi:10.1063/1.370176.
Pike, C. R., A. P. Roberts, M. J. Dekkers, and K. L. Verosub (2001), An investigation of multi-domain hysteresis mechanisms using FORC diagrams, *Phys. Earth Planet. Inter.*, *126*(1–2), 11–25, doi:10.1016/S0031-9201(01)00241-2.
Preisach, F. (1935), Über die magnetische Nachwirkung, *Z. Phys.*, *94*, 277–302, doi:10.1007/BF01349418.
Press, W. H., B. P. Flannery, S. A. Teukolsky, and W. T. Vetterling (1992), *Numerical Recipes in FORTRAN 77: The Art of Scientific Computing*, 2nd ed., 933 pp., Cambridge Univ. Press, Cambridge.
Rave, W., K. Fabian, and A. Hubert (1998), Magnetic states of small cubic particles with uniaxial anisotropy, *J. Magn. Magn. Mater.*, *190*, 332–348, doi:10.1016/S0304-8853(98)00328-X.
Roberts, A. P., C. R. Pike, and K. L. Verosub (2000), First-order reversal curve diagrams: A new tool for characterizing the magnetic properties of natural samples, *J. Geophys. Res.*, *105*(B12), 28,461–28,475, doi:10.1029/2000JB900326.
Roshko, R. M., and C. Viddal (2004), Interpreting remanence isotherms: A Preisach-based study, *Eur. Phys. J. B*, *40*(2), 145–151, doi:10.1140/epjb/e2004-00253-3.
Shaw, J. (1974), A new method of determining the magnitude of the palaeomagnetic field: Application to five historic lavas and five archaeological samples, *Geophys. J. R. Astron. Soc.*, *39*, 133–141.
Shcherbakov, V. P., B. E. Lamash, and N. K. Sycheva (1995), Monte-Carlo modeling of thermoremanence acquisition in interacting single-domain grains, *Phys. Earth Planet. Inter.*, *87*, 197–211, doi:10.1016/0031-9201(94)02969-I.
Sholpo, L. Y. (1967), Regularities and methods of study of the magnetic viscosity of rocks, *Izv. Acad. Sci., USSR Phys. Solid Earth*, Engl. Transl., *6*, 390–399.
Spinu, L., I. D. Borcia, A. Stancu, and C. J. O'Connor (2001), Time and temperature-dependent Preisach models, *Physica B*, *306*(1–4), 166–171, doi:10.1016/S0921-4526(01)00998-X.
Stancu, A., and L. Spinu (1998), Temperature- and time-dependent Preisach model for a Stoner-Wohlfarth particle system, *IEEE Trans. Magn.*, *34*(6), 3867–3875, doi:10.1109/20.728296.
Stoleriu, L., and A. Stancu (2006), Using experimental FORC distribution as input for a Preisach-type model, *IEEE Trans. Magn.*, *42*(10), 3159–3161, doi:10.1109/TMAG.2006.880112.
Stoner, E. C., and E. P. Wohlfarth (1948), A mechanism of magnetic hysteresis in heterogeneous alloys, *Philos. Trans. R. Soc. London, Ser. A*, *240*, 599–642, doi:10.1098/rsta.1948.0007.
Thellier, E. (1941), Sur la vérification d'une méthode permettant de déterminer l'intensité du champ magnétique terrestre dans la Passé, *C. R. Hebd. Seances Acad. Sci.*, *212*, 281–283.
Thellier, E., and O. Thellier (1959), Sur l'intensité du champ magnétique terrestre dans le passé historique et géologique, *Ann. Geophys.*, *15*, 285–376.
Walton, D., J. Share, T. C. Rolph, and J. Shaw (1993), Microwave magnetization, *Geophys. Res. Lett.*, *20*, 109–111, doi:10.1029/92GL02782.
Williams, W., M. E. Evans, and D. Krása (2010), Micromagnetics of paleomagnetically significant mineral grains with complex morphology, *Geochem. Geophys. Geosyst.*, *11*, Q02Z14, doi:10.1029/2009GC002828.
Wohlfarth, E. P. (1984), The coefficient of magnetic viscosity, *J. Phys. F Met. Phys.*, *14*, L155–L159, doi:10.1088/0305-4608/14/8/005.
Xu, S., and D. J. Dunlop (2004), Thellier paleointensity theory and experiments for multidomain grains, *J. Geophys. Res.*, *109*, B07103, doi:10.1029/2004JB003024.
Zijderveld, J. D. A. (1967), A. C. demagnetization of rocks: Analysis of results, in *Methods in Palaeomagnetism*, edited by D. W. Collinson, K. M. Creer, and S. K. Runcorn, pp. 254–286, Elsevier, Amsterdam.

D. Heslop, Research School of Earth Sciences, Australian National University, Canberra ACT 0200, Australia.
A. R. Muxworthy, Department of Earth Science and Engineering, Imperial College London, South Kensington Campus, London, SW7 2AZ, UK. (adrian.muxworthy@imperial.ac.uk)